3D mmW Wireless Channel Model and Its Performance Analysis for 5G

Saddam Hossain[1], Dr. Md. Abu Bakar Siddiqui[2]

[1]Dept. of Electrical & Electronic Engineering, American International University-Bangladesh (AIUB)
[2]Assistant Professor, Dept. of Electrical & Electronic Engineering, American International University - Bangladesh (AIUB)

Abstract: *To implement the three dimensional millimeter wave (3D mmW) statistical channel models, some channel parameters are required to be estimated such as temporal multipath delays, multipath power delay profiles (PDP), and multipath angle of arrival (AOA) and angle of departure (AOD). In accordance, this paper presents a 3D mmW channel model and its impulse response (IR) for LOS and NLOS link between UE and BS in urban scenario. This proposed model developed using time cluster–spatial lobe (TCSL) approach is based on 3GPP-like stochastic IR channel model. TCSL supplements the existing 3GPP-like stochastic IR channel model. This modified statistical model provides the additional channel parameters of directional RMS lobe angular spreads and RMS delay spreads for time clusters and spatial lobes (TCSLs). This proposed 3D mmW channel model can generate 3D mmW temporal and spatial channel parameters for arbitrary mmW carrier frequency, antenna beamwidth, and signal bandwidth for directional antennas. This channel model is suitable for 5G wireless communication systems.*
Keywords: *Millimeter Wave (mmW), 3D, 5G, Impulse Response (IR) model, Time Cluster (TC), Spatial Lobe(SL), Time Cluster Spatial Lobe (TCSL), Power Delay Profile (PDP).*

I. Introduction

Today's cellular systems with multiple-input multiple-output (MU-MIMO) use ultrahigh frequency and beyond [1]. As cellular providers endeavor to deliver high quality, low latency video and multimedia as well as all upcoming innovative applications for wireless devices, they are limited to a carrier frequency spectrum. A new channel model is badly needed that will be validated for operation at higher frequencies and that will allow accurate performance evaluation of possible future technical specifications. Therefore, it is extremely important to move up to millimeter wave (mmW) in order to meet the incredible demand of broadband wireless services. The next generation of wireless communications will use systems operating from 500 MHz to 100 GHz [2]. A number of mmW bands are currently being considered for global 5G networks. The Federal Communications Commission has already taken necessary steps to issue new rulemakings to bring these bands into service [3]. The 28 GHz and 73 GHz frequency bands are attractive for outdoor communications because the attenuation loss caused from atmospheric absorption is insignificant (much less than 0.1 dB) over a realistic mmW cell radius of 200 m [4],[5]. The IR channel model is first developed for four distinct frequency scenarios (i) the 28-GHz non-line of sight (NLOS) urban channel; (ii) the 73-GHz NLOS urban channel; (iii) the combined 28–73-GHz urban line of sight (LOS) channel; and (iv) the combined 28–73-GHz urban NLOS channel.

Based on mmW for 5G, many popular statistical and analytical channel models have been designed from which 3GPP, WINNER II, COST 2100, MiWEBA, METIS models and NYU WIRELESS [4] are remarkable. 3GPP and WINNER II are our main concern to design our proposed model because of the geometry based stochastic 3GPP and WINNER II spatial channel models (SCMs) [6], [7]. These models follow a system-level approach and suitable for link-level or system-level simulations to estimate realistic channels between a BS and user equipments (UEs), that account for empirical correlations between large-scale parameters. The large-scale parameters denote the omnidirectional RMS delay spread (DS), the azimuth spread (AS), the shadow fading (SF), and the Rician K-factor (for LOS channels). It's to be noted that the 3GPP and WINNER models adopt different terminologies to refer to a group of traveling multipaths. The 3GPP model defines a *path* as a time-delayed multipath copy of the transmitted signal that is subdivided into 20 rays [8], where all rays have the same path delay but slight AOD and AOA offsets. In contrast, the WINNER II model defines a *cluster* as a propagation path diffused in space, either or both in delay and angle domains, and a number of rays (typically 20) constitute a cluster, where the two strongest clusters are subdivided into three subclusters with intra-cluster delays of 0, 5, and 10 ns [9]. Current 3GPP and WINNER [9]. models make the presumption that clusters are characterized by a joint delay-angle probability density function, such that a group of traveling multipaths must depart and arrive from a unique AOD-AOA angle combination centered around a mean propagation delay [10].

Thus, this work presents a statistical spatial channel model (SSCM) developed using the time cluster–spatial lobe (TCSL) approach, which augments the existing UHF 3GPP model through the additional model parameters of directional RMS lobe angular spreads [11] for spatial lobes. Two principal units of propagation are considered in this work such as time cluster and spatial lobe, which represent the two major parts of the temporal (i.e., omnidirectional) and spatial components of this proposed statistical channel model. The TC approach has not been considered in current 3GPP and WINNER models. The SSCM presented here is based on extensive propagation measurements carried out from 2011 through 2015 by different organizations and this model generates multipath parameters for omnidirectional and directional channel impulse responses (CIRs) for links between a transmitter (TX) and receiver (RX). This paper also demonstrates that this proposed 3D mmW channel model can be generalized to arbitrary environments and antenna beamwidths to create directional channel IR in 100 GHz frequency bands.

II. 3D mmW Joint Temporal Spatial Channel Parameters

Here, we generalize the channel impulse response as a function of time, as well as a function of AOD and AOA azimuth/elevation angles, allowing realistic simulations of directional transmissions at both the TX and RX in azimuth and elevation dimensions. The omnidirectional impulse response between TX and RX is written as [12]:

$$h_{omni}\left(t,\vec{\Theta},\vec{\Phi}\right) = \sum_{n=1}^{N}\sum_{m=1}^{M_n} a_{m,n} e^{j\,\varphi_{m,n}}.\delta\left(t-\tau_{m,n}\right).\delta\left(\vec{\Theta}-\vec{\Theta}_{m,n}\right).\delta\left(\vec{\Phi}-\vec{\Phi}_{m,n}\right). \tag{1}$$

where t denotes absolute propagation time,

$\vec{\Theta} = (\theta,\phi)_{TX}$ is the vector of azimuth and elevation AODs, and $\vec{\Phi} = (\theta,\phi)_{RX}$ is the vector of azimuth and elevation AOAs; N and M_n denote the number of time clusters (TCs) and the number of cluster subpaths (SPs), respectively; $a_{m,n}$ is the magnitude of the mth SP belonging to the nth TC; $\varphi_{m,n}$ and $\tau_{m,n}$ are the phases and propagation time delays, respectively; $\vec{\Theta}_{m,n}$ and $\vec{\Phi}_{m,n}$ are the azimuth/elevation AODs and azimuth/elevation AOAs, respectively, of each multipath component. Note that a SP is an individual multipath component contained in either a SL or TC.

The omnidirectional CIR can further be partitioned to yield *directional* PDPs at a desired TX-RX unique antenna pointing angle, and for arbitrary TX and RX antenna patterns [12]:

$$h_{dir}\left(t,\vec{\Theta}_d,\vec{\Phi}_d\right) = \sum_{n=1}^{N}\sum_{m=1}^{M_n} a_{m,n} e^{j\,\varphi_{m,n}}.\delta\left(t-\tau_{m,n}\right).g_{TX}\left(\vec{\Theta}_d-\vec{\Theta}_{m,n}\right).g_{RX}\left(\vec{\Phi}_d-\vec{\Phi}_{m,n}\right). \tag{2}$$

where $\left(\vec{\Theta}_d,\vec{\Phi}_d\right)$ are the desired TX-RX antenna pointing angle, $g_{TX}\left(\vec{\Theta}\right)$ and $g_{RX}\left(\vec{\Phi}\right)$ are the arbitrary 3-D (azimuth and elevation) TX and RX complex amplitude antenna patterns of multi-element antenna arrays, respectively. In (2), the TX and RX antenna patterns amplify the power levels of all multipath components lying close to the desired pointing direction, while effectively setting the power levels of multipath components lying far away from the desired pointing direction to 0.

The statistical channel model also produces the joint AOD-AOA power spectra $P = \left(\vec{\Theta},\vec{\Phi}\right)$ in 3-D obtained by integrating the magnitude squared of equation (1) over the propagation time dimension [12],

$$P\left(\vec{\Theta},\vec{\Phi}\right) = \int_0^\infty \left|h_{omni}\left(t,\vec{\Theta},\vec{\Phi}\right)\right|^2 dt \tag{3}$$

$$P\left(\vec{\Theta},\vec{\Phi}\right) = \sum_{n=1}^{N}\sum_{m=1}^{M_n} \left|a_{m,n}\right|^2.\delta\left(\vec{\Theta}-\vec{\Theta}_{m,n}\right).\delta\left(\vec{\Phi}-\vec{\Phi}_{m,n}\right). \tag{4}$$

III. Time Clusters and Spatial Lobes Statistics

The two principal units of propagation considered in this work are a time cluster and a spatial lobe, which represent the two major parts of the temporal (i.e., omnidirectional) and spatial components of this ultimate statistical channel model. The TC approach has not been considered in current 3GPP and WINNER models. The definition of TC here considers multipath components traveling close in time, but that can arrive from many lobe angular directions, whereas current 3GPP and WINNER models assume that SPs belonging to a cluster travel along the same propagation path, but arrive at the *same* time delay over a certain AOA angular spread.

A time cluster is defined as a group of cluster subpaths (i.e., multipath components) traveling close in time and space. A time cluster is further represented by some principal cluster parameters: the absolute time of arrival at the receiver, the azimuth/elevation angles of departure, the azimuth/elevation spreads of departure, the azimuth/elevation angles of arrival, and the azimuth/elevation spreads of arrival.

A spatial lobe is defined as a departing or incoming direction of contiguous energy over the azimuth and/or elevation planes. A spatial lobe is identified by eight principal lobe parameters: the azimuth/elevation angles of departure, the azimuth/elevation spreads at the transmitter, the azimuth/elevation angles of arrival, and

the azimuth/elevation spreads at the receiver. The diagrams below illustrate time cluster and spatial lobe terminologies.

Fig.1 illustrates the combined spatial and temporal definitions described above. Initially, two clusters are transmitted from the TX at Position 1. Each cluster arrives at the receive antenna via different propagation paths to Position 2. The first (Y) arriving time cluster comes from one reflected propagation path and breaks up into two microscopic subpaths, and the second (R) arriving time cluster is composed of three cluster subpaths.
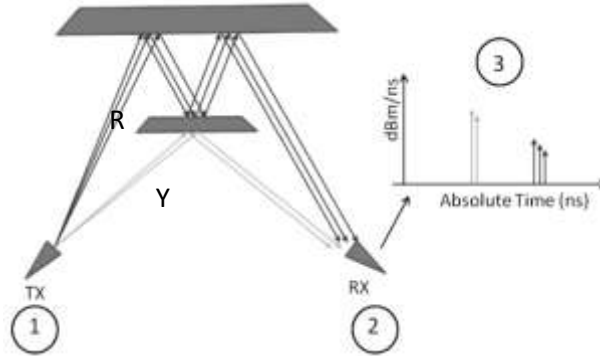

Fig. 1: Diagram illustrating two traveling time clusters leaving the same narrowbeam transmit antenna and arriving at the same narrowbeam receive antenna (i.e., same AOA).

It is important to recognize that, although both clusters arrive at the same receive angle, they each have different propagation delays. This paper describes 3-D azimuth and elevation channels where the TCSL framework models the directionality of the channels through separate TCs that have time-delay statistics, and through SLs which represent the strongest directions of multipath arrival and departure .

Table-I: TC and SL model parameters are necessary to generate 3D mmW channel impulse responses (CIRs), shown in the table.

| TC/SL	Symbol	Parameters	Distribution	Step#
TC	N	Number of time clusters	Discrete Uniform[1,6]	Step 6
	M_n	Number of Subpaths	Discrete Uniform[1,30]	Step 7
	τ_n, P_n	Cluster Delays, Powers	Exponential, Lognormal	Step 9 & 10
	$\rho_{m,n}, \Pi_{m,n}$	Subpath Delays, Powers	Exponential, Lognormal	Step 8 & 11
	$\varphi_{m,n}$	Subpath Phases	Uniform(0,2π)	Step 12
SL	L	Number of Spatial Lobes (AOD, AOA)	Poisson	Step 6
	θ, ϕ	Lobe Az./El. Angles (AOD & AOA)	Uniform (0,360), Gaussian	Step 13 & 14
	$\sigma_\theta, \sigma_\phi$	RMS Lobe Az/El. Spreads (AOD & AOA)	Gaussian, Laplacian	Step 15
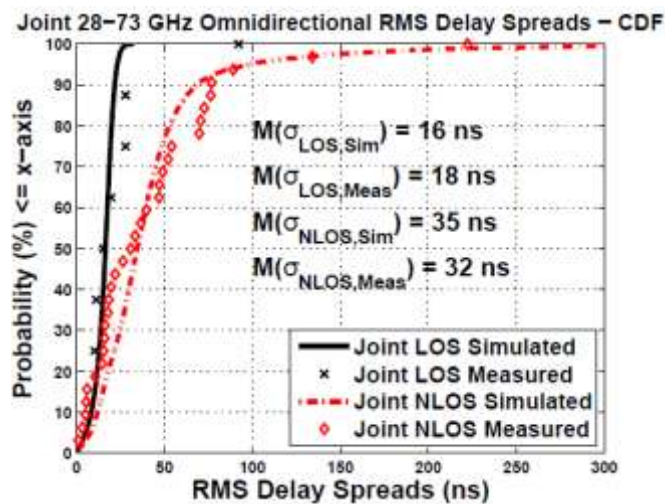
Fig. 2: Combined 28 - 73 GHz LOS and NLOS omnidirectional RMS delay spreads synthesized from absolute timing PDPs, superimposed with 10,000 simulated RMS delay spreads from generated omnidirectional PDPs [5].

IV. Generating The Temporal and Spatial 3D mmW Channel Parameters

1. Steps to create Channel Coefficients

Step 1: Set up the simulation environment (e.g. UE and BS location, antenna array configurations, building and foliage locations between UE and BS).

Step 2: Choose a propagation condition, LOS or NLOS, based on blockage between the UE and BS. Probability of LOS depends on Tx-Rx separation distance and height of UE and Tx. NYU LOS probability model can be considered to determine the probability of Line-of-Sight Link, developed by NYU [13]:

$$p(d) = \left(min\left(\frac{d_1}{d}, 1\right)\left(1 - e^{-d/d_2}\right) + e^{-d/d_2}\right)^2 \tag{5}$$

Where, d is the distance between Tx-Rx, d_1 and d_2 are the direct and bounced link distance between Tx and Rx. D_1 and d2 can be optimized by fitting a given set of data. In terms of mean square error (MSE), NYU (squared) had the lowest MSE compared to (The University of Texas at Austin) UT-Austin data set.

Step 3: Generate the Tx-Rx separation distance d (in 3D) herein we ranging from 30 to 200 m:
d=U(d_{min}, d_{max}) (6)
where we consider as,

$$\begin{cases} d_{min} = 30\ m, d_{max} = 70\ m, & LOS \\ d_{min} = 70\ m, d_{max} = 200\ m, & N\ LOS \end{cases}$$

We used the distance ranges in step 3 to validate our simulation, other distances can be valid for standards works.

Step 4: Calculate the omni-directional path loss as:

$$PL(d)[dB] = PL_{FS}(d_0) + 10n_{pl} \log_{10}\left(\frac{d}{d_0}\right) + \chi_\sigma \tag{7}$$

$$PL_{FS}(d_0) = 20 \log_{10}\left(\frac{4\pi d_0}{\lambda}\right) \tag{8}$$

Where λ is the carrier wavelength, n_{pl} is the path loss exponent (PLE) (i.e. n = 1.9 for UMi-Street Canyon-LOS, n = 3.19 for UMi-S.C.-NLOS), χ_σ describes the random shadow fading or log normal random variable with 0-mean and stander deviation σ (i.e. SF = 3.1 dB for UMi-S.C.-LOS, SF = 8.2 dB for UMi-S.C.-NLOS, d is the distance in meters, d_0 =1 m close-in (CI) free space reference distance PL model [13]. and the parameters are variant to carrier frequency and can be applied across the 6-100 GHz band.

Step 5: Generate the total omnidirectional received power P_r (dB) at the Rx location according to the environment type:
$$P_r(d)[dBm] = P_t[dBm] - PL(d)[dB] \tag{9}$$
Where P_t is the transmitted power in dBm.

Step 6: Generate the number of time clusters (TCs) N and the number of Angle of Departure (AOD) and Angle of Arrival (AOA), spatial lobes (SLs) (i.e. LAOD, LAOA) at the transmitter and Rx location [12]:
N ~ DU[1, 6]
$$L_{AOD} \sim min\{L_{max}, max\{1, Poisson(\mu_{AOD})\}\} \tag{10}$$
$$L_{AOA} \sim min\{L_{max}, max\{1, Poisson(\mu_{AOA})\}\} \tag{11}$$

Where, (L_{AOD},L_{AOA}) must always remain less than or equal to N, since the number of spatial lobes must be at most equal to the number of traveling time clusters in the channel. where μ_{AOD} = 1.6 and μ_{AOA} = 1.7 are the mean number of AOD and AOA lobes observed in Manhattan, respectively, and Lmax = 5 is the maximum allowable number of lobes, for both AODs and AOAs. The 28 GHz NLOS measurements found the maximum number of clusters N_{max} = 5 based on measurements in [11], while at 73 GHz we found N_{max} =6, therefore we use N_{max} = 6 for 100 GHz frequency band.

Step 7: Generate the number of cluster subpaths (SP) M_n in each time cluster:
$$M_n \sim DU[1, 30], \quad n = 1, 2, \dots, N \tag{12}$$

Where maximum number of cluster SPs are 30 chosen for uniform distribution for all frequencies. While, the maximum and second to maximum number of cluster subpaths are 53 and 30 respectively for 28 GHz in NLOS, over all locations, while it is 30 at 73 GHz.

Step 8: Generate the intra-cluster subpath excess delays $\rho_{m,n}$ in nanoseconds units:

$$\rho_{m,n}(b_{BB}) = \left\{ \frac{1}{b_{BB}} \times (m-1) \right\}^{1+X_n}, \quad m = 1,2,\dots\dots,M_n, \quad n = 1,2,\dots\dots,N \tag{13}$$

where $b_{BB} = 400$ MHz is the baseband bandwidth of our transmitted PN sequence (and can be modified for different baseband bandwidths), X is uniformly distributed between 0 and 0.43, and m = 1, 2, ...Mn, n = 1, 2, ...N . This step allows for a minimum subpath time interval of 2.5 ns, while reflecting our observations that the time intervals between intra-cluster subpaths tend to increase with time delay. The bounds on the uniform distribution for X will likely differ depending on the site-specific environment, and can be easily adjusted to fit field measurement observations.

Step 9: Generate the cluster excess delays τ_n (ns):
$$\tau_n'' \sim Exp(\mu_\tau) \tag{14}$$
$$\Delta\tau_n = sort(\tau_n'') - min(\tau_n'') \tag{15}$$
$$\tau_n = \begin{cases} 0 & n = 1 \\ \tau_{n-1} + \rho M_{n-1} + \Delta\tau_n + 25, & n = 2,\dots,N \end{cases} \tag{16}$$

where *sort (·)* orders the delay elements τ_n'' from smallest to largest, and where μ_τ is 123 for LOS and 83 for NLOS. This step assures no temporal cluster overlap by using a 25 ns minimum inter-cluster void interval, which was found to match the measured data, and makes sense from a physical standpoint, since multipath components tend to arrive in clusters at different time delays over many angular directions, most likely due to the free space air gaps between reflectors (buildings, lampposts, streets, etc).

Step 10: Generate TC powers P_n (mW):
$$P_n' = \overline{P_0} e^{-\frac{\tau_n}{\Gamma}} 10^{\frac{Z_n}{10}} \tag{17}$$
$$P_n = \frac{P_n'}{\sum_{k=1}^{k=N} P_k'} \times P_r \ (mW) \tag{18}$$
$$Z_n \sim N(0, \sigma_Z), \quad n = 1, \cdots, N \tag{19}$$

where $\overline{P_0}$ is the average power in the first arriving TC, Γ is the cluster decay time constant, and Z_n is a lognormal random variable with 0-dB mean and standard deviation σ_Z (e.g. 1, 3). P_n ensures that the sum of cluster powers adds up to the total omnidirectional received power *Pr.*

Step 11: Generate the cluster subpath powers $\Pi_{m,n}$ (mW) :
$$\Pi_{m,n}' = \overline{\Pi}_0 e^{-\frac{\rho_{m,n}}{\gamma}} 10^{\frac{U_{m,n}}{10}} \tag{20}$$
$$\Pi_{m,n} = \frac{\Pi_{m,n}'}{\sum_{k=1}^{k=N} \Pi_{k,n}'} \times P_n \ (mW) \tag{21}$$
$$U_{m,n} \sim N(0, \sigma_U),$$
$m = 1,2,...,M_n$ and $n = 1,2,..... N.$

where $\overline{\Pi}_0$ is the average power in the first received intra-cluster SP, γ is the SP decay time constant, and $U_{m,n}$ is a lognormal random variable with 0-dB mean and standard deviation σ_U (i.e. 6 for both LOS and NLOS) ; $\Pi_{m,n}$ ensures that the sum of SP powers adds up to the cluster power. For model validation, the SP path losses were thresholded at 180 dB (maximum measurable path loss [3]. Note that the measurements have much greater temporal and spatial resolution than previous models. Intra-cluster power levels were observed to fall off exponentially over intra-cluster time delay [12].

Step 12: Generate the cluster subpath phases $\varphi_{m,n}$(rad):
$$\varphi_{m,n} = U(0,2\pi) \tag{22}$$
where $m = 1,....,M_n$; $n = 1,2,,,, ,N.$

Different from [12] where phases are estimated from frequency and delays, here the SP phases are assumed uniform between 0 and $2\pi \cdots$ since each SP may experience a different scattering environment, thus arriving at arbitrary AOA SL.

Step 13: Recover absolute time delays $t_{m,n}$(ns) of cluster subpaths using the T-R Separation distance d using step-3:

$$t_{m,n} = t_o + \tau_n + \rho_{m,n}, \qquad (23)$$

Where, $t_o = \frac{d}{c}$, m=1,2,..... M_n, n = 1,2,,,, ,N and c=3×10^8m/s is the speed of light in free space.

Step 14: Generate the mean AOA and AOD azimuth angles θ_i(°) of the 3-D spatial lobes to avoid overlap of lobe angles [10]:

$$\theta_i \sim U(\theta_{min}, \theta_{max}) \quad i = 1,2, \cdots\cdots L \qquad (24)$$
$$\theta_{min} = \frac{360(i-1)}{L} \text{ and } \theta_{max} = \frac{360i}{L}) \qquad (25)$$

Step 15: Generate the mean AOA and AOD elevation angles of the ϕ_i(°)3-D spatial lobes (SLs):

$$\phi_i \sim N(\mu, \sigma), \quad i = 1,2, \cdots\cdots, L. \qquad (26)$$

Positive and negative values of ϕ_i indicate a direction above and below horizon, respectively. Thus , we specify (μ, σ) = $(-4.9°, 4.5°)$ for AOD elevation angles, and (μ, σ) = $(3.6°, 4.8°)$ for AOA elevation angles for all frequency scenarios are extracted from 73 GHz NLOS [14] measurements, mmWave transceivers will most likely beamform in the strongest directions with these elevation angles.

Step 16: Generate the AOD angles ($\theta_{m,n,AOD}$, $\varphi_{m,n,AOD}$)and AOA angles ($\theta_{m,n,AOA}$, $\varphi_{m,n,AOA}$) of each SP component using the SL angles found in Step 14 & 15 [14]:

$$\theta_{m,n,AOD} = \theta_i + (\Delta\theta_i)_{m,n,AOD} \qquad (27)$$
$$\phi_{m,n,AOD} = \phi_i + (\Delta\phi_i)_{m,n,AOD} \qquad (28)$$
$$\theta_{m,n,AOA} = \theta_j + (\Delta\theta_j)_{m,n,AOA} \qquad (29)$$
$$\phi_{m,n,AOA} = \phi_j + (\Delta\phi_j)_{m,n,AOA} \qquad (30)$$
$$\textit{Where, i~DU[1, L_{AOD}], j~DU[1, L_{AOA}]} \qquad (31)$$
$$(\Delta\theta_i)_{m,n,AOD} \sim N(0, \sigma_{\theta,AOD}) \qquad (32)$$
$$(\Delta\phi_i)_{m,n,AOD} \sim N(0, \sigma_{\phi,AOD}) \qquad (33)$$
$$(\Delta\theta_j)_{m,n,AOA} \sim N(0, \sigma_{\theta,AOA}) \qquad (34)$$
$$(\Delta\phi_j)_{m,n,AOA} \sim Laplace(0, \sigma_{\phi,AOA}) \qquad (35)$$

In this step, each multipath component is assigned into a single spatial AOD and AOA lobe in a uniform random fashion, in addition to a random angular offset within the SL with distributions specified in (32)–(35). Note that the 3GPP model uses a uniform distribution from −40° to +40° to generate path azimuth AODs, and for path azimuth AOAs uses a zero-mean normal distribution whose variance is a function of path powers for the UMi scenario . The WINNER models use a Normal distribution to generate path AODs and AOAs, while the Laplace distribution in (35) provided a better fit to all data across frequencies and environments than a normal distribution.

Table-II: 3D mmW Channel Model Parameters

Parameters	Simulation Values	Possible Range of Values
Operating Frequency	100 GHz	1-100 GHz
Radio Frequency (RF) Bandwidth (BW)	800 MHz	0-800 MHz
Scenario	UMa	Umi & UMa
Environment	NLOS	LOS & NLOS
T-R Separation Distance	397.9 m for NLOS, 484.8 m for LOS	10-500 m
Tx Power	30 dBm	0-30 dBm
Number of Rx Locations	5	Variable as User Density
Tx Array Type	ULA	ULA or URA
Rx Array Type	ULA	ULA or URA
Number of Tx Antenna Elements	8	Based on MIMO types
Number of Rx Antenna Elements	8	Based on MIMO types
Tx Antenna Spacing	0.5 (in Wavelength)	(0.1-100)
Rx Antenna Spacing	0.5 (in Wavelength)	(0.1-100)
Tx Antenna Azimuth HPBW	10°	7°-360°
Tx Antenna Elevation HPBW	7°	7°-45°
Rx Antenna Azimuth HPBW	7°	7°-360°
Rx Antenna Elevation HPBW	7°	7°-45°

Sample Omni. PDP Output Function

Fig.3. Simulated PDP of 100-GHz NLOS.

3-D AOD Power Spectrum - 100 GHz,NLOS
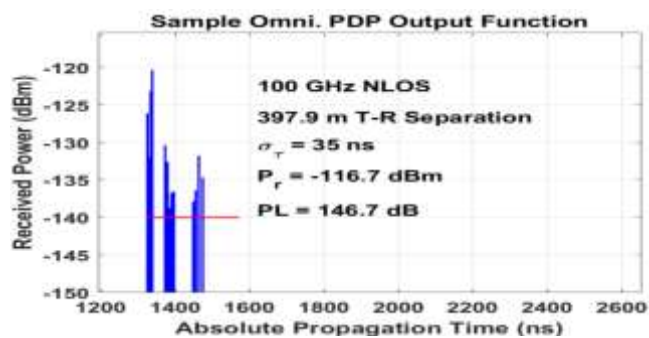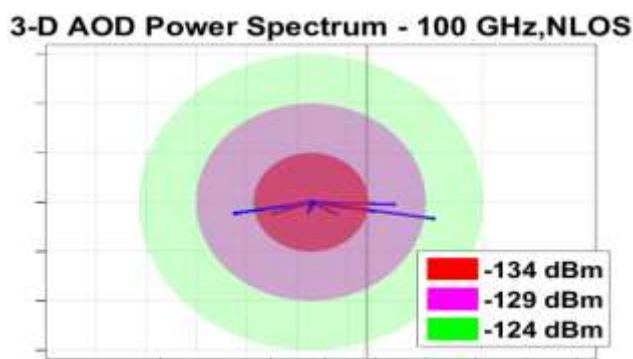

Fig.4. Simulated 100-GHz NLOS 3-D AOD power spectrum. This spectrum is associated with the PDP shown in Fig. 3.

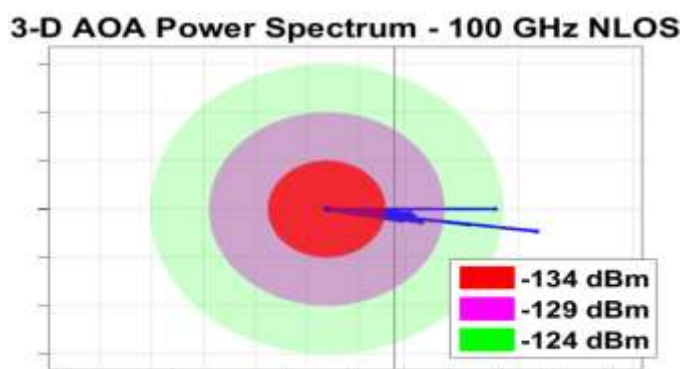**3-D AOA Power Spectrum - 100 GHz NLOS**

Fig.5. Simulated 100-GHz NLOS 3-D AOA power spectrum. This spectrum is associated with the PDP shown in Fig. 3.
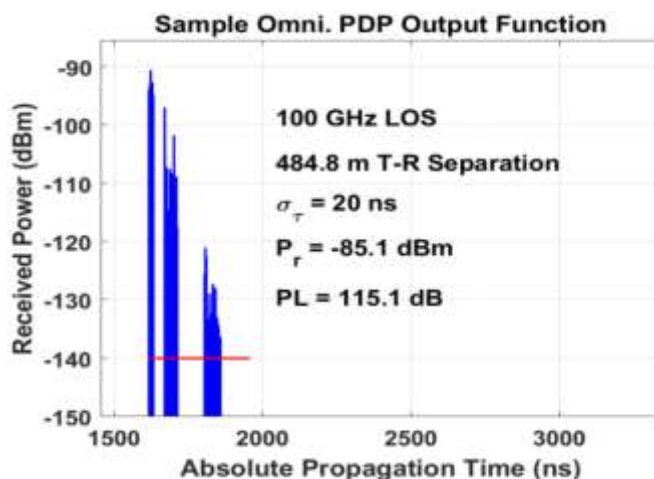
Sample Omni. PDP Output Function

Fig.6. Simulated 100-GHz LOS PDP

V. Simulation Results

Figs. 3 and 5 show the output functions of a 100-GHz NLOS omnidirectional PDP, and the corresponding AOA 3-D power spectrum, obtained from a MATLAB-based statistical simulator that implemented the channel models given in (6)–(35) using the parameters of table-II. The generated PDP in Fig. 3 is composed of thirteen multipath taps, grouped into three TCs with exponentially decaying amplitudes with cluster decay constant Γ=56.0 ns and intra-cluster SP decay constant γ= 15.3 ns (see Steps 9 and 10 in Section IV). Here, a transmit power of 30 dBm is used with a noise threshold set to −140 dBm over an 800-MHz RF bandwidth, and the simulated PDP has a total omnidirectional path loss of 146.7 dB with a TX-RX separation distance of 397.9 m, an RMS DS of 35 ns which is validated to 28 - 73 GHz LOS and NLOS omnidirectional RMS delay spreads in fig. 2, and 0-dBi TX and RX antenna gains. The AOA spectrum (Fig. 5) shows the thirteen multipath taps grouped into three AOA SLs according to (29), (30), (34), and (35) corresponding to AOD in fig. 4 . Note that the multipaths in Fig. 5 may be convolved with an arbitrary antenna pattern to study the effects of antenna beamwidths on the CIR. And Fig. 6 shows output functions of a 100-GHz LOS omnidirectional PDP where Γ=25.9 ns and intra-cluster SP decay constant γ= 16.9 ns. We used simple number generators to obtain the number of TCs, the numbers of AOD and AOA SLs, cluster and SP delays, and cluster and SP powers, as described in Section IV.

VI. Conclusion

In this paper, the statistical channel model presented in section IV is used to implement a MATLAB-based statistical simulator to verify and validate the accuracy of the simulated temporal and spatial statistics when compared against the measured statistics. The simulation was carried out for 100 GHz frequency and both LOS and NLOS scenarios presented in this work, in which many omnidirectional PDPs, and 3-D AOD and AOA power spectra were generated as sample functions of (1). This paper also shows a 3-D mmW SSCM for generating CIRs at particular distances and over local areas based on the TCSL modeling framework, which extends the 3GPP model through directional RMS lobe angular spreads while keeping consistent with the 3GPP modeling framework. The SSCM has been validated using published measurements between 28 and 73 GHz and can be used for arbitrary carrier frequency between 6 and 100 GHz (we used 100 GHz), RF signal bandwidths up to 800 MHz, and arbitrary antenna beamwidths greater than 7°. The modeling extension enables the spatial consistency in multi-user system-level simulations that account for the birth and death of time clusters (TCs) and spatial lobes (SLs) at mmW frequencies, using the statistical spatial autocorrelation for the number of TCs and SLs.

References

[1].   Lu Lu, Student Member, Geoffrey Ye Li, A. Lee Swindlehurst, Alexei Ashikhmin,Rui Zhang, '*An Overview of Massive MIMO:Benefits and Challenge*,' IEEE Journal of Selected Topics in Signal Processing, Vol. 8, No. 5, October 2014.

[2].   A white paper, '*5G Channel Model for bands up to100 GHz'* , Contributors: Aalto University-Nokia, BUPT-NTT DOCOMO, CMCC-New York University, Ericsson-Qualcomm, Huawei-Samsung, INTEL-University of Bristol, KT Corporation University of Southern California.

[3].   Theodore S. Rappaport, George R. MacCartney, Jr., Mathew K. Samimi, Shu Sun, '*Wideband Millimeter-Wave Propagation Measurements and Channel Models for Future Wireless Communication System Design'*, IEEE Transactions on Communications, Vol. 63, No. 9, September 2015.

[4].   Professor Theodore (Ted) S. Rappaport, '*Millimeter Wave Wireless Communications for 5G Cellular: It will work!'*, 2014 Personal, Indoor, and Mobile Radio Communications Conf. , Washington, DC, Sept. 5, 2014 .

[5].   M. K. Samimi, T. S. Rappaport, "Statistical Channel Model with Multi-Frequency and Arbitrary Antenna Beamwidth for Millimeter-Wave Outdoor Communications," *in 2015 IEEE Global Communications Conference, Exhibition & Industry Forum (GLOBECOM) Workshop*, Dec. 6-10, 2015.

[6].   *Spatial Channel Model for Multiple Input Multiple Output (MIMO) Simulations*, document 3GPP TR 25.996 V12.0.0, Sep. 2014.

[7].   P. Kyösti *et al.*, "WINNER II channel models," Eur. Commission, Tech. Rep. D1.1.2 V1.1, Sep. 2007.

[8].   *Spatial channel model for Multiple Input Multiple Output (MIMO) simulations* , 3GPP (RAN1) TR 25.996. (online)

[9].   P. Kyösti *et al.*, "WINNER II channel models," Eur. Commission, Tech. Rep. D1.1.2 V1.2, Sep. 2007.

[10].   Mathew K. Samimi, Theodore S. Rappaport , '*Characterization of the 28 GHz Millimeter-Wave Dense Urban Channel for Future 5G Mobile Cellular,'* NYU Polytechnic School of Engineering 2 MetroTech Center, Brooklyn, NY 11201, June 24, 2014.

[11].   Samimi, M., Wang, K., Azar, Y., Wong, G. N., Mayzus, R., Zhao, H., Schulz, J. K., Sun, S., Gutierrez, F., Rappaport, T. S., "28 GHz Angle of Arrival and Angle of Departure Analysis for Outdoor Cellular Communications using Steerable Beam Antennas in New York City," to appear in the 2013 IEEE Vehicular Technology Conference (VTC), June 2~5, 2013.

[12].   M. K. Samimi, T. S. Rappaport, "3-D Statistical Channel Model for Millimeter-Wave Outdoor Mobile Broadband Communications," *accepted at the 2015 IEEE International Conference on Communications (ICC)*, 8-12 June, 2015.

[13].   K. Haneda *et al.*, "5G 3GPP-like Channel Models for Outdoor Urban Microcellular and Macrocellular Environments," to be published in *2016 IEEE 83rd Vehicular Technology Conference (VTC 2016-Spring)*, May, 2016.

[14].   Mathew K. Samimi, Theodore S. Rappaport, '*3-D Millimeter-Wave Statistical Channel Model for 5G Wireless System Design,'* IEEE Transactions on Microwave Theory and Techniques, vol. 64, no. 7, July 2016.